Mechanisms and models of the turbulent boundary layers at transcritical conditions

Fangbo Li[*1,2,3], Weiwei Zhang[1,2,3], Matthias Ihme[*4,5]

[1]School of Aeronautic, Northwestern Polytechnical University, Xi'an 710072, China;

[2]International Joint Institute of Artificial Intelligence on Fluid Mechanics, Northwestern Polytechnical University, Xi'an, 710072, China;

[3]National Key Laboratory of Aircraft Configuration Design, Xi'an 710072, China

[4]Department of Mechanical Engineering, Stanford University, Stanford, CA 94305, USA

[5]Department of Photon Science, SLAC National Accelerator Laboratory, Menlo Park, CA 94025, USA

*Corresponding authors: fbli@nwpu.edu.cn; mihme@stanford.edu

Computational models for high-pressure transcritical turbulence in wall-modeled large-eddy simulation typically rely on wall-function models to overcome the need for resolving the boundary layer structures. However, the mechanisms and models of turbulent boundary layer at transcritical conditions remain poorly understood since the near-wall flow and heat transfer are significantly affected by the enhanced fluctuations and steep gradients in thermodynamic properties. To address this issue, we study the mechanisms of transcritical turbulent boundary layers and wall-attached models at transcritical conditions. It is shown that the real-fluid variable-property effects are associated with the coupling between the near-wall cycle and the wall-normal coherent motions in the outer layer, resulting in the amplification of turbulent energy in the outer layer and noticeable energy transfer between the log-layer and the outer layer; hence, turbulence in the log-layer is modulated by the outer layer. Based on this underlying physical principle, we propose the characteristic velocity and length scales for the

attached eddy at transcritical conditions, and extend the attached eddy model to transcritical turbulent boundary layers by introducing a mixed scaling that incorporates both inner and outer scalings. We show that the new characteristic scales and extended attached-eddy model perform well in characterizing the structures in transcritical turbulent boundary layers.

I. INTRODUCTION

At supercritical pressures, the thermodynamic properties of fluids differ from those at subcritical conditions. Transitioning from the liquid-like phase to gas-like phase regions, which is called "transcritical conditions", can occur without the formation of the interface [1]. Under transcritical conditions, all the thermodynamic and transport properties, including density, viscosity, specific heat capacity and thermal conductivity, vary significantly across the Widom line, introducing significant real-fluid thermodynamic effects [2-7]. Variations in thermodynamic and transport properties of the fluids under transcritical conditions can lead to substantially modified turbulence statistics and structural behaviors when compared to wall-bounded flows at subcritical pressures [3-5, 8-11]. In particular, momentum and energy transfer in the turbulent boundary layer of transcritical wall-bounded flows have a substantial impact on turbulent structural properties and modeling.

Improving the accuracy of wall-modelled large-eddy simulations (WMLES) for predicting transcritical flows requires the inspections of the characteristics of turbulent boundary layers at these conditions since the performance of the wall-function model greatly depends on the properties of the logarithmic layer. To provide theoretical support to the development of wall models for simulating transcritical flows, specific focus is thereby directed towards the statistical and structural properties in the turbulent boundary layers. According to the classical description of incompressible turbulent boundary layers [12-13], the near-wall turbulence consists of locally active motions (u_i) and inactive

motions (u_o), where u_i denotes the inner-flow-induced motions characterized by the inner scaling (velocity scale u_τ and length scale δ_v) and u_o is the outer-flow-induced motions that scale with outer-layer parameters (velocity scale u_τ and length scale L_y, with L_y being the half-height of the channel). Here, $u_\tau = \sqrt{\tau_w / \rho_w}$ is the friction velocity and $\delta_v = \mu_w / (\rho_w u_\tau)$ is the viscous lengthscale, where τ_w is the wall shear stress, μ is the dynamic viscosity, ρ is the fluid density and subscript w denotes the value at the wall. The typical structures in low-*Re* wall-bounded turbulence are the coherent structures with the streamwise length of ~$1000\delta_v$ and spanwise spacing of ~$100\delta_v$ [14-15] in the viscous sublayer and the buffer layer. For moderate and high *Re* turbulence, Zhao and Smith [12] conducted experiments to obtain the streamwise and wall-normal turbulence components in incompressible pipe flows; they found that the wall-normal spectra collapse in the energy-containing region with inner scaling, but a ζ/R (with ζ the wall distance and R the pipe radius) dependence was observed for the low-wavenumber region, implying the effects of the outer flow on the near-wall motions. Simultaneous streamwise velocity measurements within the incompressible turbulent boundary layer at high Reynolds numbers were conducted by Guala *et al*. [13]. Their results showed that the signature of large-scale structures can be found within the wall region and that these scales interact with the near-wall turbulence, which appears to be a primary difference to low-*Re* turbulence. The interactions in turbulent boundary layer are generally accompanied with the turbulent energy transport in turbulent boundary layers. With regard to the interactions in turbulent boundary layer, two mechanisms, namely “bottom-up” [16-20] and “up-bottom” [21-23], were reported. Lee and Moser [24] analyzed DNS data of channel flows with Re_τ = 930, and showed that the large-scale structures in the outer layer, resulting from the structures with streamwise lengths less than 3δ (with δ the height of turbulent boundary layer) in the buffer layer, extend beyond 3δ in the streamwise direction. Furthermore, the experiments on turbulent

boundary layers with Re_τ = 1060 by Ganapatosubramani *et al.* [25] showed that the large-scale structures have streamwise length of 1.5δ at ζ/δ = 0.1; while at ζ/δ = 0.5, their streamwise length reduces to 0.6δ, suggesting that turbulent energy transform from the inner layer to the outer layer (i.e., "bottom-up" mechanism). However, the spectral analysis by Wang and Zheng [26] implied that the premultiplied spectra in low-*Re* boundary layers decreases with ζ, while the spectra of the low wavenumber region in high-*Re* boundary layers increase with ζ, implying the "up-bottom" mechanism of energy transfer [26].

The inner-outer interactions influence the dynamics in turbulent boundary layers by means of modulating the organizations of wall-attached eddies [27-28]. The wall-attached eddy hypothesis [29] is a structural model for the incompressible turbulent boundary layer. This model indicates that in turbulent boundary layers, the dominant momentum-carrying motions are organized into a multiscale population of eddies attached to the wall. A growing body of theoretical, experimental and numerical studies have supported that these self-similar energy-containing eddies have significant impact on the energy transfer and statistical profiles in the logarithmic region [29-33]. Under the hypothesis that the self-similar structures result in the linearly growing mixing length and logarithmic mean velocity in the logarithmic layer, Townsend [29] developed a theoretical attached-eddy model that predicts the wall-normal distributions of fluctuating velocity in the logarithmic layer. This attached eddy model was extended in incompressible flows by a series of studies [34-37]. According to this model, the velocity fluctuations at a generic location in the log-layer result from a superposition of the velocities induced by different attached eddies at that location, implying that the statistical behaviors in the log-layer may result from the interactions between the inner-layer and the outer-layer motions. For incompressible flows, the eddies are assumed to be inviscid and a slip boundary condition is applied

at the wall [29, 32]. Currently, the wall-attached eddy has been reported in studies covering a wide range of Reynolds numbers (Re_τ = 546 in Ref. [31]; Re_τ = 1000 in Ref. [32]; Re_τ = 500 ~ 20000 in Ref. [38]; Re_τ = 2000 ~ 1.4×10^6 in Ref. [39]; Re_τ = 186 ~ 934 in Ref. [40]; Re_τ = 1000 ~ 5200 in Ref. [41]). Another critical issue for the attached eddy investigation is the velocity and length scales of the eddies, which characterize the scales of the energy-containing structures in boundary layers [31, 40]. The classical attached eddy theory shows that the turbulent velocity is characterized by u_τ, while the length scale of the eddies is the distance to the wall since the log-layer motions are too large to be affected by viscosity but small compared to the boundary-layer limit $O(L_y)$ [29, 31]. Recently, Lozano-Durán & Bae [31] modified the characteristic scales of attached eddy for incompressible flows with Re_τ = 546 by assuming that the momentum-carrying eddies are controlled by the mean momentum flux and mean shear. The efforts on identifying the characteristics scales of turbulent structures are also helpful for establishing the algebraic mixing-length model, which can be used as the wall model in WMLES methodology.

For turbulent boundary layers with variable thermal properties, Patel *et al.* [42] and Patel, Boersma & Pecnik [43] reported that the statistical profiles, near-wall streaks, and anisotropy are significantly modulated by the variable density and viscosity in the channel. However, the semilocal scaling that considers mean density variations is still effective and as a result, statistics maintain similarity in the cases with the same semilocal Reynolds number Re_τ^* ($\mathrm{Re}_\tau^* = \overline{\rho} u_\tau^* L_y / \overline{\mu}$, with u_τ^* the semilocal friction velocity, $u_\tau^* = \sqrt{\tau_w / \overline{\rho}}$) [42-44]. At transcritical conditions, the variations in thermophysical properties become more pronounced and many studies found that the semilocal scaling fails to collapse the statistical profiles in different cases [4, 8-9, 11]. The deficiency of classical scaling laws at transcritical conditions results from the peculiar structural dynamics of turbulent boundary layers

under real-fluid thermodynamic effects. Instantaneous visualizations of transcritical boundary layers [3, 6, 11] showed that the dense fluids ejected from the core cause positive density skewness in the buffer layer region. In addition, the velocity fluctuations correlated with the near-wall streak structures in the transcritical heated turbulent boundary layers alter the generation of mean-density- and density-fluctuation-related Reynolds shear stresses in the buffer layer and the log-layer [45]. Peeters *et al.* [10] also found that the variations in density and viscosity affect the vortical dynamics in the viscous sublayer and the buffer layer; the thermal expansion related to the density changes at transcritical conditions contributes to the transport of streamwise vortices.

The above review on transcritical turbulence shows that the real-fluid variable-properties at transcritical conditions result in peculiar organizations of near-wall turbulent streaks and coherent structures. However, the features and physical models for the attached eddy at transcritical conditions remain unclear. Although the attached eddy hypothesis was supported by the inverse wavenumber scaling for energy spectra and logarithmic scaling for structure function in transcritical turbulent boundary layer [3-4], the characteristics related to the attached eddy at transcritical conditions have not yet been reported. As in Cheng and Fu [27], the inner-outer interactions and the attached eddy model are quantitatively consistent in incompressible turbulent boundary layer even at low and moderate *Re*, the velocity fluctuations and turbulent stress generated by inner-outer-interaction in turbulent boundary layers follow the predictions made by the attached eddy theory. With this in mind, we can hypothesize that the inner-outer interactions originating within the turbulent boundary layers have significant effects on the attached eddies. The objective of the present study is to elucidate the structural behaviors of transcritical wall-bounded flows, with the primary innovation being the substantiation of the inner-outer interactions in the turbulent boundary layers with strong variations in

thermodynamic properties. Moreover, we also extend the attached eddy model [29, 35-36] to transcritical flows and provide new scaling for the wall-attached eddy model by considering the inner-outer interactions in turbulent boundary layers.

The remainder of this paper is organized as follows. Sec. II introduces our DNS methodology and database for transcritical channel flows. Sec. III is associated with results of turbulent structures and attached eddy model in transcritical boundary layers. Finally, the concluding remarks are given in Sec. IV.

II. DNS DATABASE OF TRANSCRITICAL CHANNEL FLOWS

In this study, we analyze the turbulent boundary layers from an existing DNS database of the transcritical isothermal channel flows established in our prior studies [3-6]. The present working fluid is nitrogen with the critical pressure p_c = 3.3958 MPa and the critical temperature T_c = 126.19 K. For the transcritical isothermal channel, the temperatures for the hot wall and the cold wall are kept spatially and temporally constant. The flow domain is of size L_x (streamwise) × $2L_y$ (wall-normal) × L_z (spanwise), with $L_x/L_y = 2\pi$, $L_z/L_y = 4\pi/3$, and with channel half-height L_y = 0.045 mm. The flow has a bulk pressure of p_b = 3.87 MPa (corresponding to a reduced pressure of p_r = 1.14) and is driven by a streamwise body force so that the mass flow rate is kept constant. The streamwise, wall-normal and spanwise coordinates are defined over the ranges $0 \le x \le L_x$, $-L_y \le y \le L_y$ and $0 \le z \le L_z$, respectively.

We use the cubic Peng-Robinson (PR) equation [46] as the equation of state (EoS) for transcritical nitrogen. Peng-Robinson (PR) equation reads

$$p = \frac{\rho RT}{1-b\rho} - \frac{\rho^2 a}{1+2b\rho-b^2\rho^2}, \tag{1}$$

where R is the gas constant and the parameters a and b are given as

$$a = 0.457236\frac{R^2T_c^2}{p_c}\left[1+c\left(1-\sqrt{\frac{T}{T_c}}\right)\right]^2, \tag{2}$$

$$b = 0.077796\frac{RT_c}{p_c}, \tag{3}$$

with

$$c = 0.37464 + 1.54226\omega - 0.26992\omega^2, \tag{4}$$

and with $\omega = 0.04$ being the acentric factor. For N_2, $b = 8.58\times10^{-4}$ and $c = 0.432$. All thermodynamic quantities are derived using the appropriate departure functions [3-6]. The transport properties (dynamic viscosity μ and thermal conductivity λ) are evaluated by the model for high-pressure fluids [47]. These models for thermal properties have been employed with their accuracy examined in our previous works [3-6].

In this study, we present results for four cases, i.e., TR3, TR1.9, TR1.4 and TR1. These cases are summarized in Table I. The reader is referred to Refs. [3-6] for the details on the DNS configurations, methodology, validations and mesh convergence analysis. Here we only make a briefly introduction. Cases TR3, TR1.9, TR1.4 are transcritical with a reduced temperature of $T_{r,\,cold} = 0.79$ at the cold wall. In case TR1, the two reduced wall temperatures are the same at 0.79, resulting in a constant-property incompressible flow with negligible heat transfer. The domain is discretized using a structured grid with mesh size $N_x \times N_y \times N_z = 384 \times 256 \times 384$. Expressed in wall units, the resolution corresponds to $\Delta x^+ = 4.9 \sim 8$, $\Delta z^+ = 3.26 \sim 6.8$, $\Delta y^+ = 0.29 \sim 0.47$ at the cold wall and $\Delta y^+ = 0.2 \sim 1$ at the hot wall. After the flow reaches a statistically steady state, we average over homogenous directions and time over more than ten flow-through times to obtain statistically-converged results; one flow-through time is defined as $L_x / \overline{u_b}$ with $\overline{u_b}$ being the bulk velocity.

Case	$T_{r,\,cold}$	$T_{r,,\,hot}$	$\rho_{r,\,cold}$	$\rho_{r,\,hot}$	$Re_{\tau,\,cold}$	$Re_{\tau,\,hot}$	ρ_{cold}/ρ_{hot}
TR3	0.79	2.38	2.17	0.12	430	300	18
TR1.9	0.79	1.51	2.17	0.22	440	610	10
TR1.4	0.79	1.11	2.17	0.42	500	1370	5.2
TR1	0.79	0.79	2.17	2.17	700	700	1

TABLE I. Summary of boundary conditions of all DNS cases. The subscripts *hot* and *cold* indicate the conditions at the hot wall and the cold wall, respectively.

III. RESULTS AND DISCUSSIONS

In this section, we discuss the results. The Reynolds-averaged Navier-Stokes (RANS) mean of any variable f is defined here as $\overline{f}$, and its perturbation from the mean is denoted by f'. The density-weighted (Favre) average of f is obtained by computing $\tilde{f} = \overline{\rho f} / \overline{\rho}$, and f'' is the corresponding perturbation. $\overline{f}$ and $\tilde{f}$ represent averages in the streamwise direction x_1 and spanwise direction x_3.

A. Interactions in the turbulent boundary layers at transcritical conditions

To study the interactions within turbulent boundary layers, we compute the linear coherence spectrum (LCS), a parameter reflecting the linear coupling between fluctuations of different near-wall structures, to examine the spectral coherence between a near-wall reference position ζ_r in the log-layer and different wall-normal locations ζ in the outer layer of turbulent boundary layers [48]. To account for the density variations at transcritical conditions, we replace the fluctuating velocity in the classical LCS definition [48] with the density-weighted fluctuating velocity, as shown in Eq. (5):

$$\gamma_L^2(\zeta,\zeta_r,\lambda_x) = \frac{\left|\overline{\hat{\phi}(\zeta,\lambda_x)\hat{\phi}^{\#}(\zeta_r,\lambda_x)}\right|^2}{\left|\hat{\phi}(\zeta,\lambda_x)\right|^2\left|\hat{\phi}(\zeta_r,\lambda_x)\right|^2} = \frac{\left|E'_{\rho uu}(\zeta,\zeta_r,\lambda_x)\right|^2}{E_{\rho uu}(\zeta,\lambda_x)E_{\rho uu}(\zeta_r,\lambda_x)}, \tag{5}$$

where $\hat{\phi}$ is the density-weighted streamwise fluctuating velocity ($\phi = \sqrt{\rho}u$) in Fourier space, $\hat{\phi}^{\#}$

is its complex conjugate, ζ_r is the reference wall-normal position and λ_x is the streamwise wavelength. In Fig. 1, we present the linear coherence spectrum between ζ_r^* = 50 (the reference position in the log-layer, ζ^* is the semilocal wall units, $\zeta^* = \bar{\rho} u_\tau^* \zeta / \bar{\mu}$) and ζ^* = 300 in the outer layer for all cases. The results clearly show that $\gamma^2_{L,\mathrm{TR3}} > \gamma^2_{L,\mathrm{TR1.9}} > \gamma^2_{L,\mathrm{TR1.4}} > \gamma^2_{L,\mathrm{TR1}}$, indicating an enhancement in spectral coherence between the log-layer and the out layer with increasing real-fluid thermodynamic effects. When using the semilocal viscous lengthscale δ_v^* to rescale λ_x, we find that γ_L^2 first increases, then keeps nearly unchanged with increasing λ_x, implying that stronger spectral coherence exists for large-scale structures. The increasing spectral coherence clearly suggests that the interactions between the log-layer and the outer layer for transcritical turbulent boundary layers. We will then confirm this by examining the energy transfer in transcritical turbulent boundary layers.

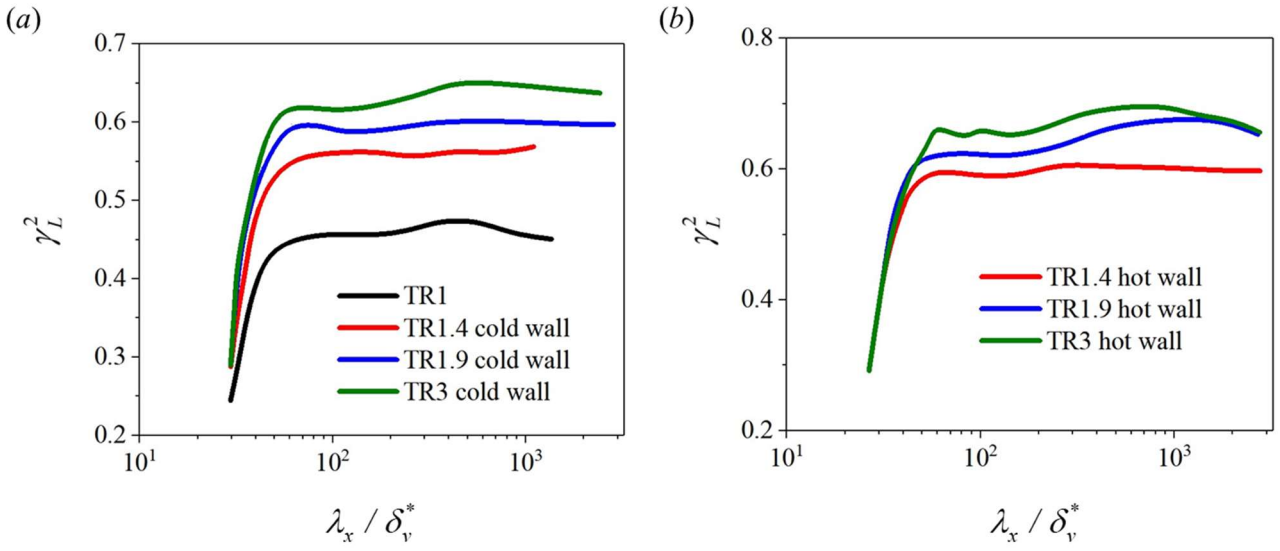

FIG. 1. The LCS of the density-weighted streamwise velocity between ζ_r^* = 50 (in the log-layer) and ζ^* = 300 (in the outer layer): (a) near the cold wall; (b) near the hot wall. The streamwise wavenumber λ_x is rescaled by δ_v^* at ζ^* = 300.

The inner-outer interactions are further substantiated by means of sweep and ejection motions. Fig. 2 shows the results of quadrant analysis [5, 45] for the streamwise Reynolds stresses $\rho u'' u''$. Here, the

streamwise Reynolds stresses are decomposed into four quadrant events, and the contributions to the streamwise Reynolds stresses from each quadrant as a function of ζ^* are presented. The quadrants represent the following turbulent motions:

i) Near the cold wall: Q1 events with $u'' > 0$ and $v'' > 0$, Q2 events with $u'' < 0$ and $v'' > 0$ (ejection), Q3 events with $u'' < 0$ and $v'' < 0$, and Q4 events with $u'' > 0$ and $v'' < 0$ (sweep);

ii) Near the hot wall: Q1 events with $u'' > 0$ and $v'' > 0$, Q2 events with $u'' < 0$ and $v'' > 0$ (sweep), Q3 events with $u'' < 0$ and $v'' < 0$, and Q4 events with $u'' > 0$ and $v'' < 0$ (ejection).

Generally, the results show that, compared with TR1, the streamwise fluctuating energy is strengthened in the outer layer while reduced in the viscous wall-layer for transcritical cases (TR3 and TR1.9). The amplification of fluctuating energy in the outer layer may result from the energy transfer from the inner layer to the outer layer in the presence of the real-fluid thermodynamic conditions. Consequently, the interactions between the outer layer and the inner layer are strengthened. It can be seen that the streamwise turbulent stress is mainly generated by the ejection and sweep motions indicated by Q2 and Q4 events; hence, we can expect that the energy transfer within the turbulent boundary layer is accompanied with the enhancement of ejection or sweep motions in the outer layer and the attenuation of these motions in the inner layer. These will be discussed in the next section which focuses the turbulent structures that are associated with the interactions within the turbulent boundary layer at transcritical conditions.

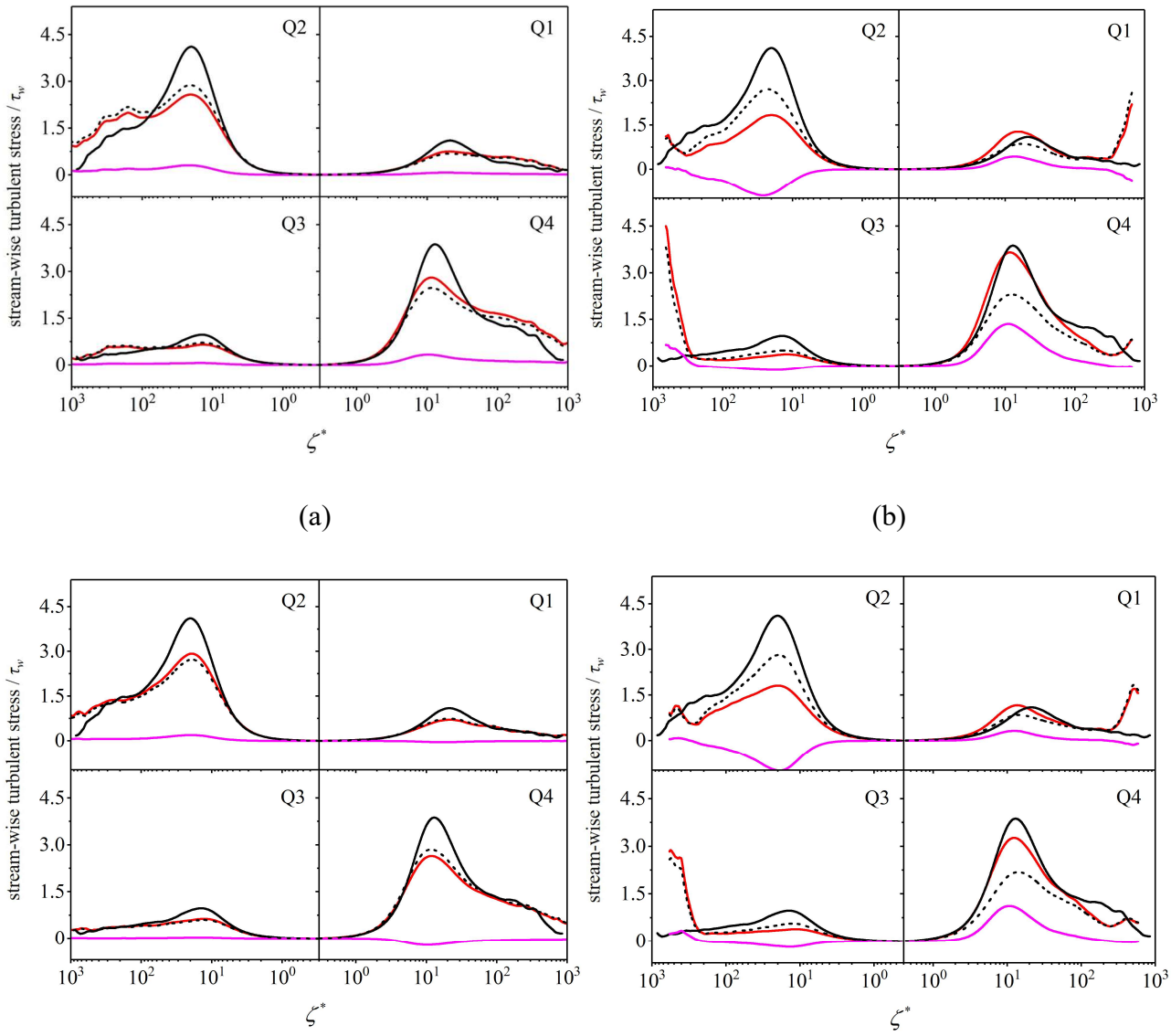

FIG. 2. Quadrant analysis on the streamwise Reynolds stress. Black lines, $\overline{\rho}\widetilde{u''u''}$ in TR1; red lines, $\overline{\rho}\widetilde{u''u''}$ in TR3 or TR1.9; dashed lines, $\overline{\rho u''u''}$ in TR3 or TR1.9; pink lines, $\overline{\rho' u''u''}$ in TR3 or TR1.9. (a) near the cold wall for TR3; (b) near the hot wall for TR3; (c) near the cold wall for TR1.9; (d) near the hot wall for TR1.9.

Finally, the interactions within the transcritical turbulent boundary layer are visualized by the near-wall turbulent structures. Fig. 3 shows the contours of density at several wall-normal locations near the hot wall for TR3, with the isocontours of wall-normal velocity fluctuations v'' included. We note

that the density and the velocity fluctuations in TR3 are well correlated. Instantaneous snapshots of the density at $\zeta^* = 540$ in the outer layer imply that the high-density regions are associated with the sweep motions indicated by $v'' > 0$ (see Fig. 3(a)). The low-density regions correspond to the ejection motion indicated by $v'' < 0$ (see Fig. 3(b)), suggesting the low-density fluids ejected from the inner layer. In contrast, at $\zeta^* = 100$ and $\zeta^* = 50$, $v'' > 0$ is associated not only with the high-density streaks but also the low-density streaks (as shown in Fig. 3(c) and Fig. 3(e)), which appears to be different from the outer layer (i.e., $\zeta^* = 540$). This peculiar phenomenon is the consequence of the near-wall cycle and the interactions between the inner and the outer layers. The streamwise vortices with low density are populated in the buffer layer, the lift-up of these vortices transport them away from the wall, and then break-up in the outer layer. The low-density streaks thereby sweep towards the wall, resulting in $v'' > 0$ associated with the low-density streaks. Significant energy transfer originates from these wall-normal coherent motions within the turbulent boundary layers since the ejection and sweep motions play a significant role in the energy transport in transcritical turbulent boundary layers.

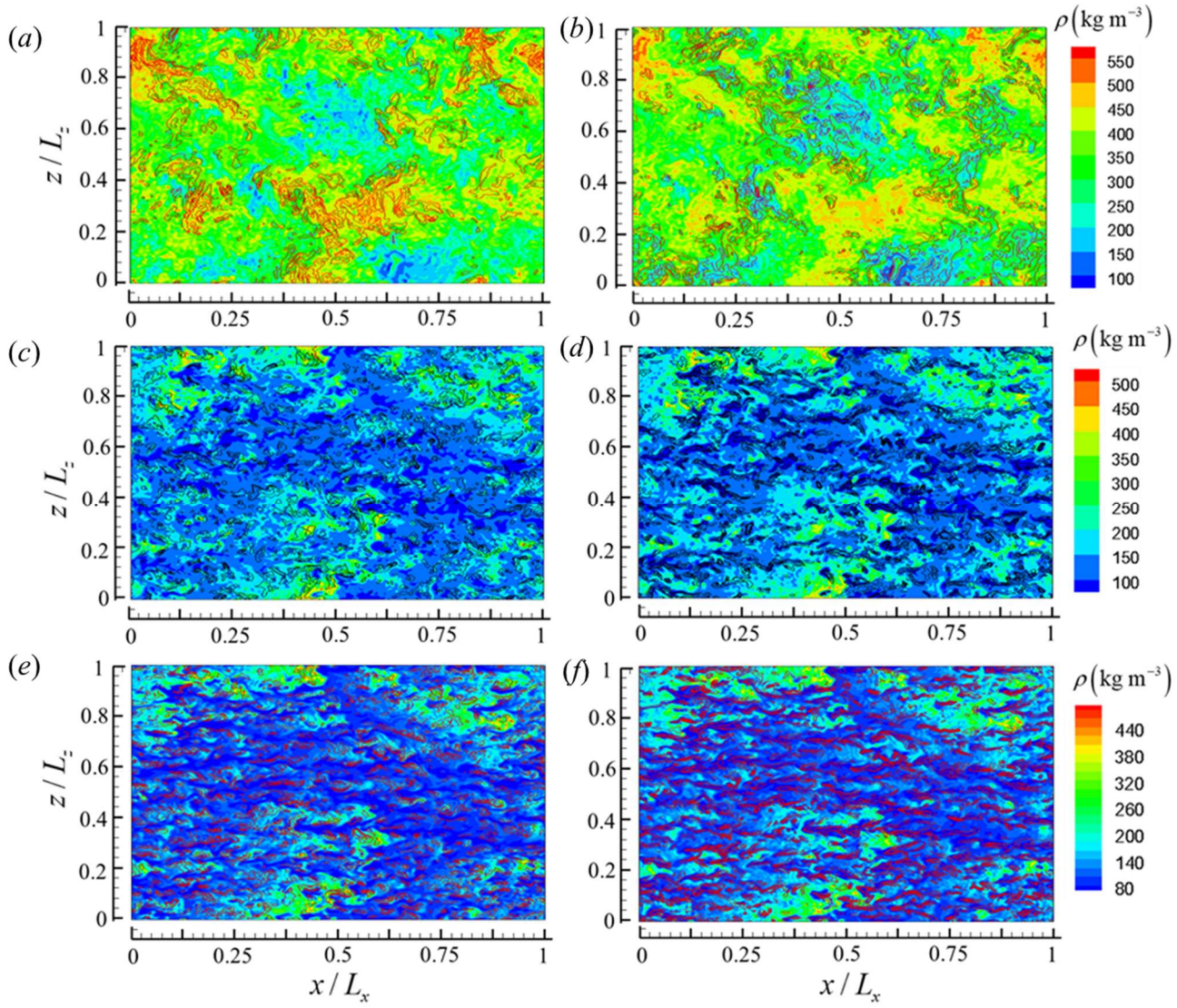

FIG. 3. Instantaneous snapshots (entire *x*-*z* plane) of the density near the hot wall of TR3, with (a ~ b), (c ~ d), (e ~ f) for $\zeta^* = 540$, 100, and 50, respectively. The superimposed lines in (a), (c), (e) indicate the positive wall-normal velocity fluctuations ($v'' > 0$), while in (b), (d), (f) the superimposed lines represent the negative wall-normal velocity fluctuations ($v'' < 0$).

For a more quantitative view of the interactions within the transcritical turbulence boundary layers, instantaneous isosurfaces of wall-normal velocity fluctuations as well as corresponding contours of density near the cold wall are shown in Fig. 4. For TR3, the isosurface of wall-normal velocity fluctuations with $v'' = 2.5\ \mathrm{m{\cdot}s^{-1}}$ and $v'' = 1.2\ \mathrm{m{\cdot}s^{-1}}$ is associated with high-density structures (typically $\rho > 550\ \mathrm{kg{\cdot}m^{-3}}$ in Fig. 4, corresponding to $\bar{\rho}$ in the buffer layer), exhibiting clear ejection events from

the near-wall layers as the near-wall turbulence lifts up the dense fluid into the lighter core of the channel. Apparently, this wall-normal mixing leads to significant interactions between the inner layer and the outer layer, resulting in effective mass transport and heat transfer in the log-layer. As the density ratio of the channel decreases, the number density of the structures with v'' = 1.2 m·s^{-1} and v'' = 2.5 m·s^{-1} decreases, implying attenuated ejection and sweep motions with decreasing density ratio in the channel. As the fluctuating density is enhanced, so are the interactions between the inner layer and the outer layer.

The isosurfaces of instantaneous density colored by the streamwise velocity fluctuations for TR3 are shown in Fig. 5, in which the range of ζ^* is $50 < \zeta^* < 500$ near both walls. In Fig. 5(a), the density $\rho = 400$ kg·m^{-3} corresponds to ζ^* = 1100 (in the outer layer) near the cold wall in the mean density profile. The structures with $\rho = 400$ kg·m^{-3} shown in Fig. 5(a) originate from the high-speed streaks ($u'' > 0$) in the outer layer, which allows one to conclude that these high-speed streaks correspond to the sweeping structures from the outer layer. Thus, the interactions between the outer layer and the log-layer are achieved by the high-speed, sweeping streaks from the outer layer. The structures with $\rho = 600$ kg·m^{-3} (corresponding to ζ^* = 17 near the cold wall for the mean density profile) have negative u'', suggesting that the high-density structures are associated with the low-speed streaks; hence, the mixing between the inner layer and the log-layer is achieved by the ejected low-speed streaks from the buffer layer. A similar analysis can be performed near the hot wall. The low-density isosurfaces of $\rho = 100$ kg·m^{-3} in Fig. 5(c) and $\rho = 300$ kg·m^{-3} and Fig. 5(d)) (corresponding to ζ^* = 26 and ζ^* = 430 near the hot wall for the mean density profile, respectively) are associated with both the low-speed streaks and the high-speed streaks. These results confirm that the interactions between the near-wall turbulence and the outer layer originate from the appearance of wall-normal motions of

these structures at transcritical conditions.

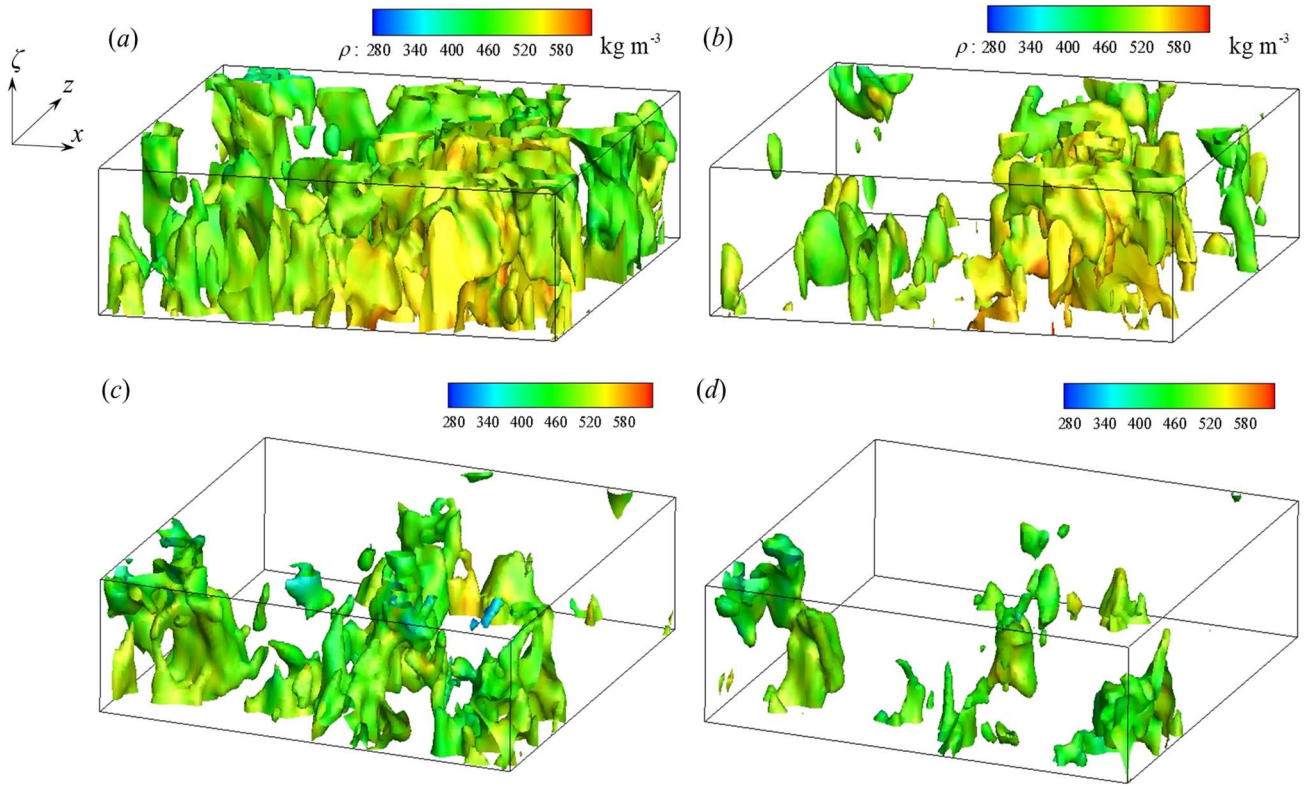

FIG. 4. Isosurfaces of wall-normal velocity fluctuation colored by the instantaneous density near the cold wall, with $v'' = 1.2$ m·s^{-1} in the left panel and $v'' = 2.5$ m·s^{-1} in the right panel. (a-b) TR3; (c-d) TR1. The wall-normal coordinates correspond to $50 < \zeta^* < 500$.

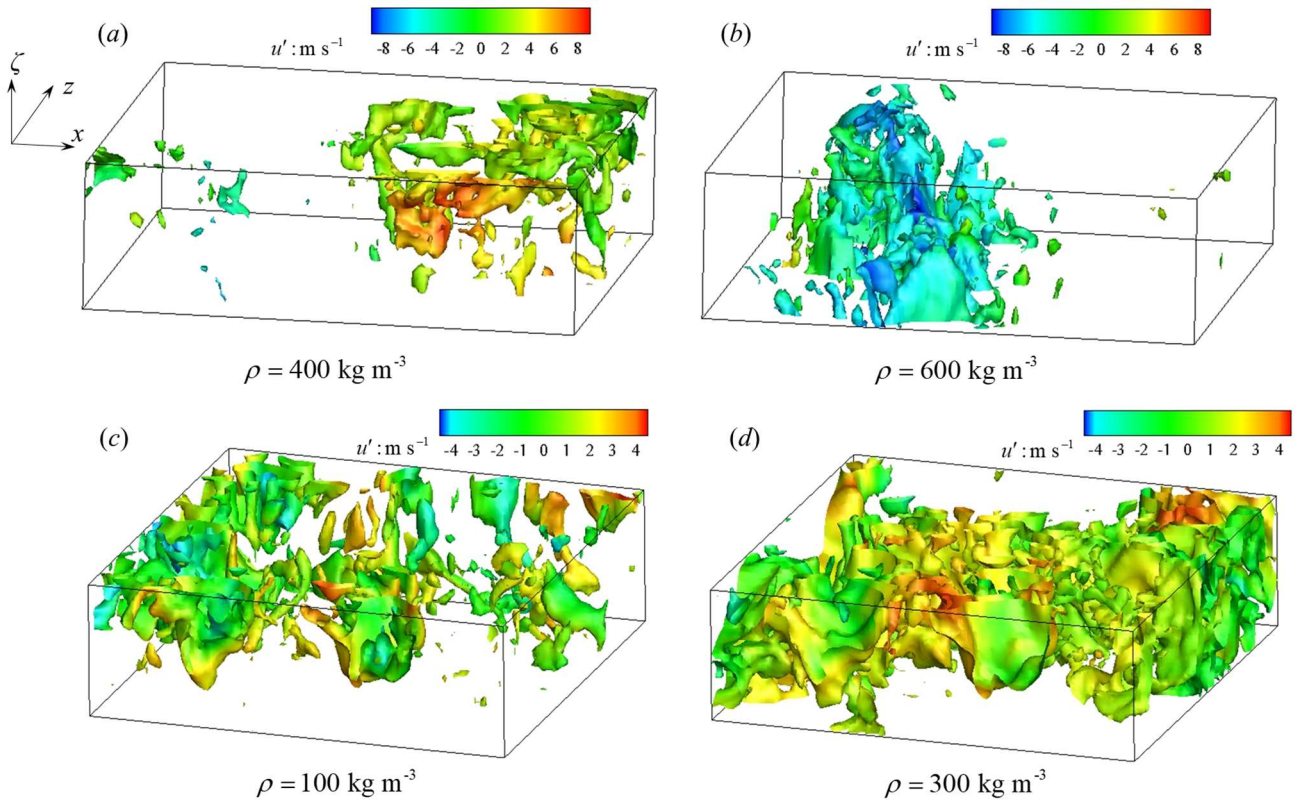

FIG. 5. Isosurfaces of instantaneous density colored by u' for TR3: (a) isosurfaces of $\rho = 400$ kg·m^{-3} near the cold wall; (b) isosurfaces of $\rho = 600$ kg·m^{-3} near the cold wall; (c) isosurfaces of $\rho = 100$ kg·m^{-3} near the hot wall; (d) isosurfaces of $\rho = 300$ kg·m^{-3} near the hot wall. The wall-normal coordinates correspond to $50 < \zeta^* < 500$.

We can summarize the interactions within the turbulent boundary layer at transcritical conditions in a schematic to provide a mechanistic description. As shown in Fig. 6, wall-normal coherent motions including sweep and ejection are enhanced at transcritical conditions. This results in the sweep of high-speed streaks and the ejection of low-speed streaks, which then leads to the interactions and energy transfer between the inner layer and the outer layer. These enhanced interactions are therefore closely associated with the changes of the characteristic scales of the attached eddies. The coupling between the near-wall cycle and the wall-normal coherent motions are also observed in the near-wall regions, thus the statistics in the log-layer are modulated by both the inner-layer motions and the outer-layer

motions. The above structural changes in turbulent boundary layers in the presence of real-fluid thermodynamic effects enable considerable coherence between the log-layer and the outer layer. Finally, the scaling merely considering the inner scaling (such as semilocal scaling) and the outer scaling cannot provide accurate predictions of the statistics in transcritical turbulent boundary layers.

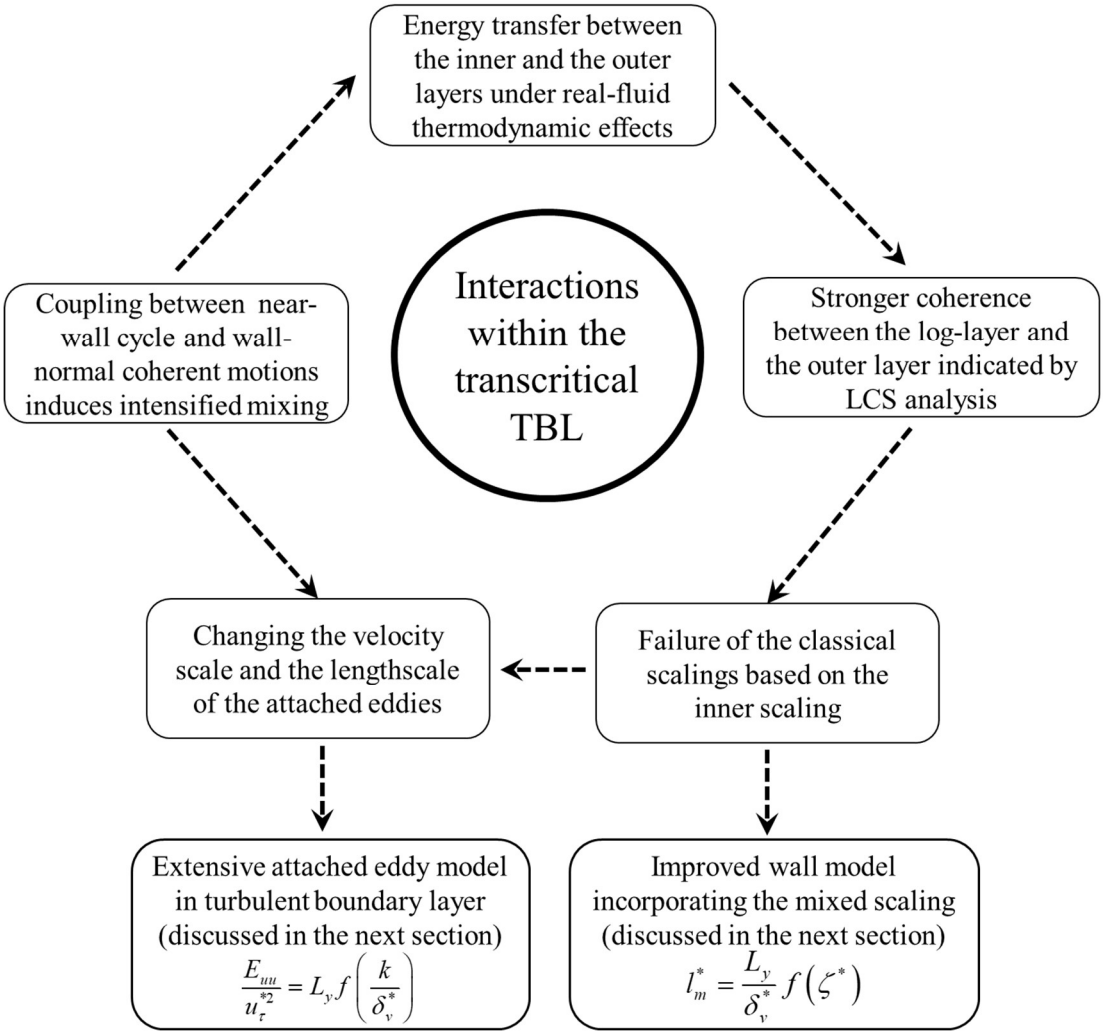

FIG. 6. A sketch of interactions within the turbulent boundary layer at transcritical conditions

B. Characteristic scales of turbulent structures at transcritical conditions

For a more quantitative view of the turbulent structures in the transcritical turbulent boundary layer, the characteristic scales of the attached eddy are examined with particular attentions given to spectra in the log-layer. The characteristic velocity scale and length scale for the attached eddy in incompressible flows (i.e., u_τ^* and ζ), the inner scaling δ_v^* and outer scaling L_y, are considered. In

Fig. 7, we extract the profiles of the energy spectra of the streamwise fluctuating velocity in different scalings. We observe that the collapse among the different profiles cannot be achieved when using u_τ^* and δ_v^* to rescale the energy spectra (see Fig. 7(a)). This is remarkably different from the conclusions drawn in variable-property turbulence [42]. The significant differences of the rescaled spectra near the hot wall and those near the cold wall when using the inner scaling u_τ^* and δ_v^* are prominent. Fig. 7(b) shows that the energy spectra normalized by characteristic scales in traditional attached eddy model, i.e., u_τ^* and ζ. No general collapse is found in any wavenumber region, suggesting that the real-fluid thermodynamic effects change the characteristics scales of the attached eddies. The interactions within the turbulent boundary layer imply that the outer scaling should be taken into consideration when developing the characteristic scales of attached eddies in transcritical flows.

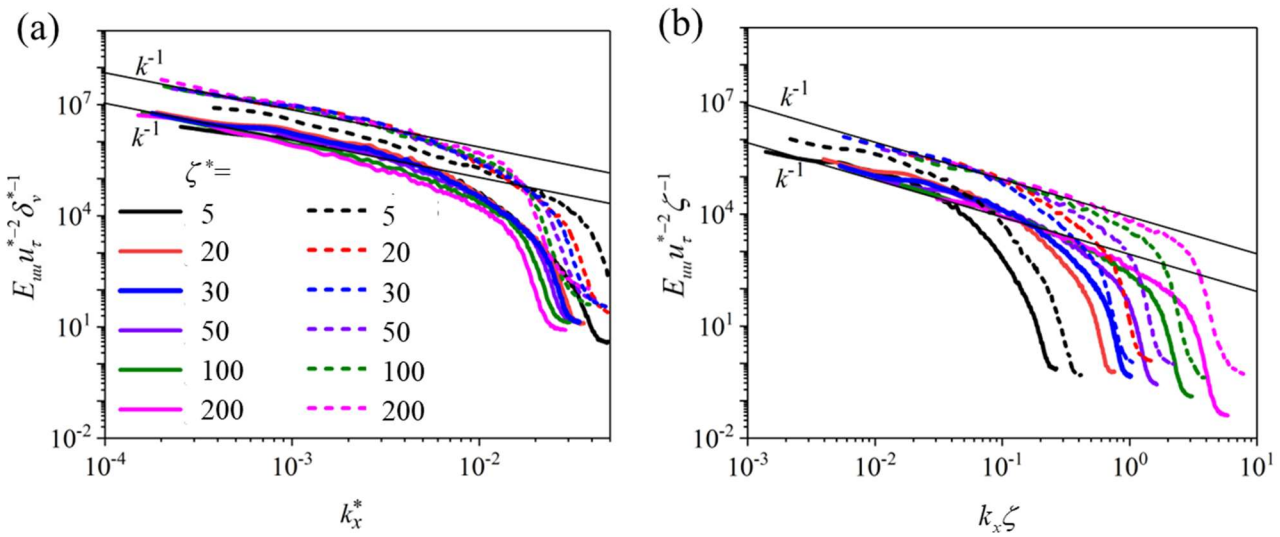

FIG. 7. Energy spectra of streamwise fluctuating velocity using inner scaling and characteristic scales in the traditional attached eddy model extracted at different wall-normal locations for TR3. (a) using u_τ^* and viscous length-scale δ_v^* (i.e., inner scaling) to rescale the energy spectra; (b) using u_τ^* and ζ (i.e., characteristic scales in the traditional attached eddy model) to rescale the energy spectra. Solid profiles: near the cold wall; dashed profiles: near the hot wall.

The mixing length is another quantity which is associated with the length scale of the attached eddies. In the log-layer of incompressible turbulent boundary layers, the mixing length is proportional to the length scale of the attached eddies. In the non-equilibrium wall models, the algebraic mixing-length model,

$$l_m = \kappa\zeta\left[1-\exp\left(\frac{\zeta^+}{A^+}\right)\right], \tag{6}$$

is commonly employed to evaluate the eddy viscosity [49], where l_m is the mixing length and $A^+ = 26$ [49]. In Fig. 8, we examine the effectiveness of Eq. (6). Fig. 8(a) shows the results of $l_m/(\kappa\zeta)$ given by Eq. (6), the profiles cannot collapse onto the exponential curve given by $1-\exp\left(-\zeta^+/A^+\right)$. Patel *et al.* [42] suggested to use semilocal scaling to collapse the statistical profiles for different variable-property wall-bounded flows. Fig. 8(b) gives the results of the semilocal mixing length for all cases. The good collapse of the cold wall profiles is observed; profiles at the cold walls are more similar in nature to the classical constant-property results, with comparatively less effect of near-wall property gradients on the mean flow. The changes and fluctuations near the hot wall for TR3 are most significant among all cases, and the profiles near the hot wall do not collapse for all cases, implying the deficiency of semilocal scaling with the increasing density fluctuations.

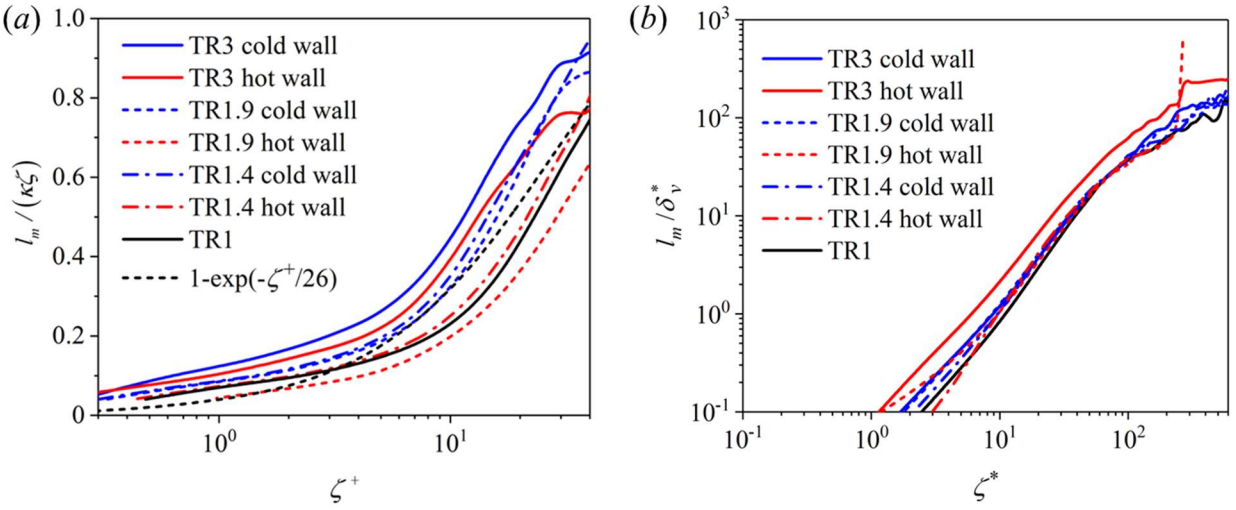

FIG. 8. Examinations on the algebraic mixing-length wall model. (a) mixing length given by Eq. (6); (b) mixing length in semilocal scaling.

Evidently, the semilocal scaling is achieved by the normalization with the inner scaling δ_v^*. The inadequacy of the semilocal scaling at transcritical conditions leads us to hypothesize that a mixed scaling that accounts for the effects of the outer scaling should be considered in turbulent boundary layers with strong variations in thermodynamic properties. According to this, we propose a new scaling for mixing length:

$$\frac{l_m}{L_y} = f\left(\frac{\zeta}{\delta_v^*}\right) = f\left(\zeta^*\right). \tag{7}$$

In Eq. (7), the mixing length is rescaled by the channel half-height L_y while the wall-normal distance is normalized by the semilocal viscous lengthscale. Eq. (7) can be transformed to the following form:

$$l_m^* = \frac{L_y}{\delta_v^*} f\left(\zeta^*\right) = \sqrt{\frac{\overline{\rho}}{\rho_w}} \frac{\overline{\mu}}{\mu_w} Re_\tau \, f\left(\zeta^*\right), \tag{8}$$

with ζ^* and l_m^* the semilocal wall distance and mixing length, respectively, $\zeta^* = \zeta / \delta_v^*$, $l^* = l_m / \delta_v^*$. Eq. (8) exposes the modification of the semilocal scaling by employing the mixed scale L_y / δ_v^*. Fig. 9(a) shows that this new scaling is effective to collapse all profiles of the mixing length onto a single curve in the log-layer. To further substantiate the effectiveness of the mixed scaling, the energy spectra scaled by the mixed scaling for all cases are examined in Fig. 9(b). Following this mixed scaling, the energy spectra are rescaled by u_τ^* and L_y, and wavenumber k is rescaled by δ_v^*, i.e.,

$$\frac{E_{uu}}{u_\tau^{*2} L_y} = f\left(k^*\right) = f\left(k\delta_v^*\right). \tag{9}$$

Compared with the results using inner scaling (Fig. 7(a)) and characteristic scales in the traditional attached eddy model (Fig. 7(b)), the mixed scaling achieves better collapse for all the profiles. For the energy containing region, the spectra for all cases can collapse reasonably well. The results of the

rescaled spectra highlight the effectiveness of the mixed scaling (Eq. (7) and Eq. (9)). Eq. (7) provides an effective way to predict the mixing length, and also provides the reduced-order mixing-length model which can be employed in WMLES methodology. Furthermore, the interactions between the inner layer and the outer layer are also confirmed by the better collapse of the energy spectra incorporating the outer scaling displayed in Fig. 9(b).

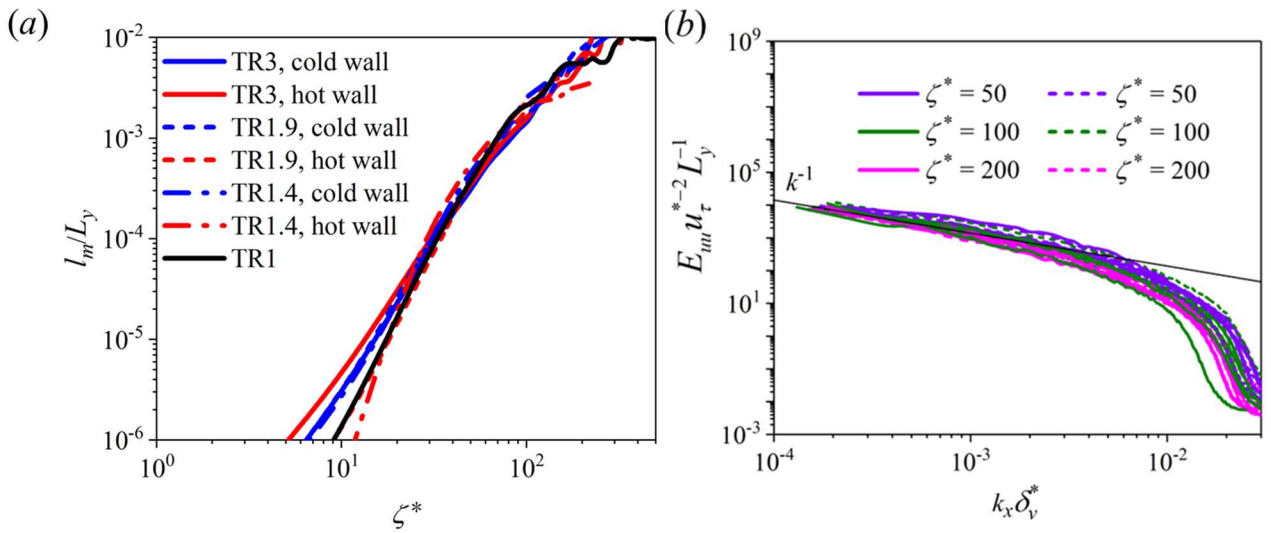

FIG. 9. Predictions of (a) the mixing length based on the mixed scaling; (b) the energy spectra normalized by the mixed scaling for all cases, the solid lines indicate the cold wall profiles and the dashed lines denote the hot wall profiles.

C. An extended attached eddy model at transcritical conditions

A key conclusion drawn from the results in Sec. III A is that for transcritical turbulent boundary layers, the log-layer is mutually modulated by the inner layer and the outer layer. Ma *et al.* [3] showed that the streamwise velocity structure function follows a logarithmic scaling and the streamwise energy spectrum exhibits an inverse wave-number scaling, providing support for the attached-eddy hypothesis at transcritical conditions. According to the hierarchical random organization of the attached eddies, the eddies are generated at the wall, the number of eddies doubles as their size halves; the eddies fill

the space from the wall to the log-layer, where neither viscous effects nor large-scale effects play a significant role [34-37]. The hierarchical random organization in the traditional attached eddy model indicates that i) the eddies are prominently influenced by the inner layer, while the influences imposed by the outer motions are inactive [12]; ii) the characteristic lengthscale of the attached eddies is the wall-normal distance ζ [29, 31]. However, the traditional attached eddy model cannot be straightforwardly extended to the transcritical turbulent boundary layer due to the existence of interactions between the inner layer and the outer layer. In this section, we establish the extended attached eddy model by introducing the mixed scaling presented in Eq. (7) and Eq. (9). Let us retain the following natures of attached eddies at transcritical conditions according to the hierarchical random additive process:

i) The attached eddies are a hierarchy of self-similar eddy motions which are inertially dominated, and attached to the wall;

ii) The attached eddies have random and independent distributions, thus it follows that the velocity fluctuations at a generic location are generated by the random superposition of all the eddy-induced velocities at that location.

Based on the self-similar characteristics of the attached eddies, the fluctuating velocity $\boldsymbol{u}'(\boldsymbol{x}) = \boldsymbol{u}'(x, \zeta, z)$ induced by a particular eddy can be given by the universal expression according to Townsend [29]:

$$\boldsymbol{u}'(\boldsymbol{x}) = u_\tau \boldsymbol{f}\left(\frac{\boldsymbol{x}-\boldsymbol{x}_a}{\zeta_a}\right), \tag{10}$$

with u_τ the friction velocity, namely, the characteristic velocity of the eddy, and $\boldsymbol{x_a} = (x_a, \zeta_a, z_a)$ is the coordinate of the center of the attached eddy. Here we extend Eq. (10) by considering the characteristic velocity of attached eddies (i.e., u_τ^*) and the mixed scaling (i.e., L_y / δ_v^*) at transcritical conditions:

$$\boldsymbol{u}'(\boldsymbol{x}) = u_\tau^* \frac{L_y}{\delta_v^*} \boldsymbol{f}\left(\frac{\boldsymbol{x}-\boldsymbol{x}_a}{\delta_v^*}\right), \tag{11}$$

or,

$$\boldsymbol{u}'^*(\boldsymbol{x}) = \frac{L_y}{\delta_v^*} \boldsymbol{f}\left(\frac{\boldsymbol{x}-\boldsymbol{x}_a}{\delta_v^*}\right). \tag{12}$$

Eq. (11) suggests the idea of improving the semilocal scaling for velocity fluctuations by the factor L_y / δ_v^*, thus showing consistency with the mixed scaling given by Eqs. (7) and (9). According to Mouri [50], the free-slip wall condition imposes $f_u \neq 0$, $f_v = 0$ and $f_w \neq 0$ at $\zeta = 0$. As justified later, in the log-layer ($\zeta \to 0$), it is reasonable to assume

$$f_u \propto \frac{g_u}{\delta_v^*},\ f_v \propto \frac{\zeta}{\delta_v^{*2}} g_v = \frac{\zeta^*}{\delta_v^*} g_v,\ f_w \propto \frac{g_w}{\delta_v^*}, \tag{13}$$

with g being some function of $(x - x_a)/\delta_v^*$ and $(z - z_a)/\delta_v^*$. Assuming that the attached eddies have a population density $P(u_\tau^*, \boldsymbol{x}_a)$ (i.e., the number density of the attached eddies per unit area of the wall), the two-point correlation of fluctuating velocity in the channel can then be determined by integrating Eq. (11):

$$\begin{aligned}\overline{\boldsymbol{u}''(\boldsymbol{x})\boldsymbol{u}''(\boldsymbol{x}+\boldsymbol{r})} &= \iint P\left(u_\tau^*, \boldsymbol{x}_a\right) u_\tau^{*2} \frac{L_y^2}{\delta_v^{*2}} \boldsymbol{f}\left(\frac{\boldsymbol{x}-\boldsymbol{x}_a}{\delta_v^*}\right) \boldsymbol{f}\left(\frac{\boldsymbol{x}+\boldsymbol{r}-\boldsymbol{x}_a}{\delta_v^*}\right) \mathrm{d}u_\tau^* \mathrm{d}\boldsymbol{x}_a \\ &= \int \left[\int P\left(u_\tau^*, \zeta_a\right) u_\tau^{*4} \mathrm{d}u_\tau^* \cdot \iint \frac{L_y^2}{\overline{V}^2} \boldsymbol{f}\left(\frac{\boldsymbol{x}-\boldsymbol{x}_a}{\delta_v^*}\right) \boldsymbol{f}\left(\frac{\boldsymbol{x}+\boldsymbol{r}-\boldsymbol{x}_a}{\delta_v^*}\right) \mathrm{d}x_a \mathrm{d}z_a \right] \mathrm{d}\zeta_a .\end{aligned} \tag{14}$$

Eq. (14) can then be equivalently written as

$$\overline{\boldsymbol{u}''(\boldsymbol{x})\boldsymbol{u}''(\boldsymbol{x}+\boldsymbol{r})} = \int \left[\int P\left(u_\tau^*, \zeta_a\right) u_\tau^{*4} \mathrm{d}u_\tau^* \right] \delta_v^{*3} \frac{L_y^2}{\overline{V}^2} \boldsymbol{I}\left(\boldsymbol{x}^*, \boldsymbol{r}^*\right) \mathrm{d}\zeta_a^*, \tag{15}$$

with $\boldsymbol{x}_a^* = \boldsymbol{x}_a / \delta_v^*$, $\zeta_a^* = \zeta_a / \delta_v^*$ and $\boldsymbol{I}\left(\boldsymbol{r}^*, \boldsymbol{x}^*\right)$ the eddy-intensity function,

$$\boldsymbol{I}\left(\boldsymbol{r}^*, \boldsymbol{x}^*\right) = \iint \boldsymbol{f}\left(\frac{\boldsymbol{x}-\boldsymbol{x}_a}{\delta_v^*}\right) \boldsymbol{f}\left(\frac{\boldsymbol{x}+\boldsymbol{r}-\boldsymbol{x}_a}{\delta_v^*}\right) \mathrm{d}x_a^* \mathrm{d}z_a^* . \tag{16}$$

The limit $\nu \to 0$ is taken so as to ignore the viscous length ν/u_τ with respect to the height ζ_a [29, 50].

Then, a free-slip condition, i.e., $u'' \neq 0$ and $w'' \neq 0$, is imposed on the wall at $\zeta = 0$ [29, 50]. In Townsend's attached eddy theory, this wall condition of velocity fluctuations yields $I_{uu} = \text{const}$ and $I_{uv} = a(\zeta / \zeta_a)$ with a a constant at $\zeta / \zeta_a \ll 1$ and $\boldsymbol{r} = 0$, reproducing the nature of constant $\overline{u''v''} / u_\tau^2$ in the log-layer (i.e., $\zeta \to 0$). Ma *et al*. [3] examined the Reynolds shear stress in the log-layer and reported that $\overline{u''v''} / u_\tau^{*2}$ keeps nearly constant in the log-layer for transcritical channel flows with $Re_\tau > 300$. At $\zeta \to 0$ and $\boldsymbol{r} = 0$. The condition of Eq. (14) yields

$$\frac{\overline{u''v''}}{u_\tau^{*2}} \propto \int \left[\int N\left(u_\tau^*, \zeta_a^*\right) u_\tau^{*4} \mathrm{d}u_\tau^* \right] \delta_v^{*3} \frac{L_y^2}{\overline{\nu}^4} \zeta_a^* \mathrm{d}\zeta_a^*, \tag{17}$$

and

$$\frac{\overline{u''^2}}{u_\tau^{*2}} \propto \int \left[\int N\left(u_\tau^*, \zeta_a^*\right) u_\tau^{*4} \mathrm{d}u_\tau^* \right] \delta_v^{*3} \frac{L_y^2}{\overline{\nu}^4} \mathrm{d}\zeta_a^*. \tag{18}$$

with $N\left(u_\tau^*, \zeta_a^*\right) = P\left(u_\tau^*, \zeta_a^*\right)\left(L_x L_z\right)$ the number of the attached eddies with the size ζ_a. Integrating Eqs. (17) and (18) shows that the Reynolds stresses at the wall-normal location ζ are generated by the superposition of the effective attached eddies (with characteristic velocity of u_τ^*) whose center coordinate ranges from ζ to L_y. According to the dimensional analysis, reproducing the constant $\overline{u''v''} / u_\tau^{*2}$ at $\zeta_a \to 0$ gives rise to the following potential expression for N:

$$N \propto \left(\zeta_a^*\right)^{-1}. \tag{19}$$

Eq. (19) implies that the population density of attached eddies exhibits inverse scaling with the wall-normal size of the eddies. According to Eq. (18), we have

$$\begin{aligned} \frac{\overline{u''^2}}{u_\tau^{*2}} &\propto \int \left[\int N u_\tau^{*4} \mathrm{d}u_\tau^* \right] \delta_v^{*3} \frac{L_y^2}{\overline{\nu}^4} \mathrm{d}\zeta_a^* \propto \int_{\zeta^*}^{L_y/\delta_v^*} \frac{1}{\zeta_a^*} u_\tau^{*5} \delta_v^{*3} \frac{L_y^2}{\overline{\nu}^4} \mathrm{d}\zeta_a^* \\ &= A_1 \ln\left(L_y / \zeta\right) + B_1, \end{aligned} \tag{20}$$

whose Fourier transformation leads directly to the celebrated inverse wavenumber scaling of the streamwise energy spectra, i.e.,

$$E_{uu} \propto k^{-1}. \tag{21}$$

The scaling of energy spectra obtained from Eq. (21) is consistent with DNS results. In addition, the dimensional analysis of $N\left(u_\tau^*,\zeta_a^*\right)$ results in the following scaling law for the number of the attached eddies:

$$N\left(u_\tau^*,\zeta_a^*\right) \propto u_\tau^{*-2}\overline{\nu}\left(\zeta_a^*\right)^{-1} = u_\tau^{*-1}\delta_\nu^*\left(\zeta_a^*\right)^{-1}. \tag{22}$$

It can be seen that when plugging Eq. (22) into Eq. (17), the constant Reynolds shear stress is recovered. This provides justification for the form of function $\boldsymbol{f}$ in Eq. (13). In appendix A, we show that the present model reduces to Townsend's wall-attached model for incompressible flows.

Finally, we show the population density of attached eddies in transcritical flows to verify the scaling (Eq. (22)). Several studies have been performed to examine the population density of attached structures for incompressible flows. Hwang and Sung [32] reported that the distribution of the attached eddies is inversely proportional to its wall-normal extent for incompressible turbulent boundary layers. Since the attached eddies can be regarded as a hierarchy of geometrically self-similar structures in turbulent boundary layers [32, 48], we adopt the clustering methodology to distinguish the attached eddy structures following Cheng *et al.* [40]. The positive attached eddies (PAE) are defined as spatially connected regions satisfying

$$u_i''\left(x,\zeta,z\right) > \alpha u_{i,rms}''\left(\zeta\right), \tag{23}$$

whereas the negative attached eddies (NAE) are regions with

$$u_i''\left(x,\zeta,z\right) < -\alpha u_{i,rms}''\left(\zeta\right). \tag{24}$$

In Eqs. (23) and (24), $u_{i,rms}''$ denotes the root-mean-square of the velocity components and α is the threshold. Cheng *et al.* [40] took α as 1.5 based on percolation theory. Fig. 10 shows the clusters of streamwise velocity fluctuations identified by Eqs. (23) and (24). We observe that the clusters of u''

have complex shapes, most of the clusters are attached to the wall whereas a few clusters distribute above the wall, exhibiting detachment from the wall. To extract the attached structures from these clusters, Cheng *et al.* [40] classified these clusters into two groups: attached eddies with the wall distance $\zeta^+ \le 1$ and detached eddies with the wall distance $\zeta^+ > 1$. In this study we follow this procedure to determine the number of the attached eddy structures. The streamwise, wall-normal and spanwise extents of the bounding box of the structures satisfying Eqs. (23) and (24) are defined as l_x, l_y and l_z. To examine the present scaling of the population density of the attached eddies in transcritical turbulent boundary layers, we show the population density of the positive and negative attached eddies as a function of ζ^* for TR3 and TR1.9 in Fig. 11. Note that since the eddies are attached to the wall, the wall-normal extent l_y of the wall-attached eddies is equivalent to ζ. It can be seen in Fig. 11 that the population density of the attached eddies (including both PAE and NAE) can be well approximated by $P \propto \left(l_y^*\right)^{-1.1}$. These results indicate that the population density of the attached structures at transcritical conditions is associated with their hierarchical length scales, with the decay of P_{AE} deviating slightly from the theoretical estimations $\left(\zeta^*\right)^{-1}$ that is given by our extended attached eddy model.

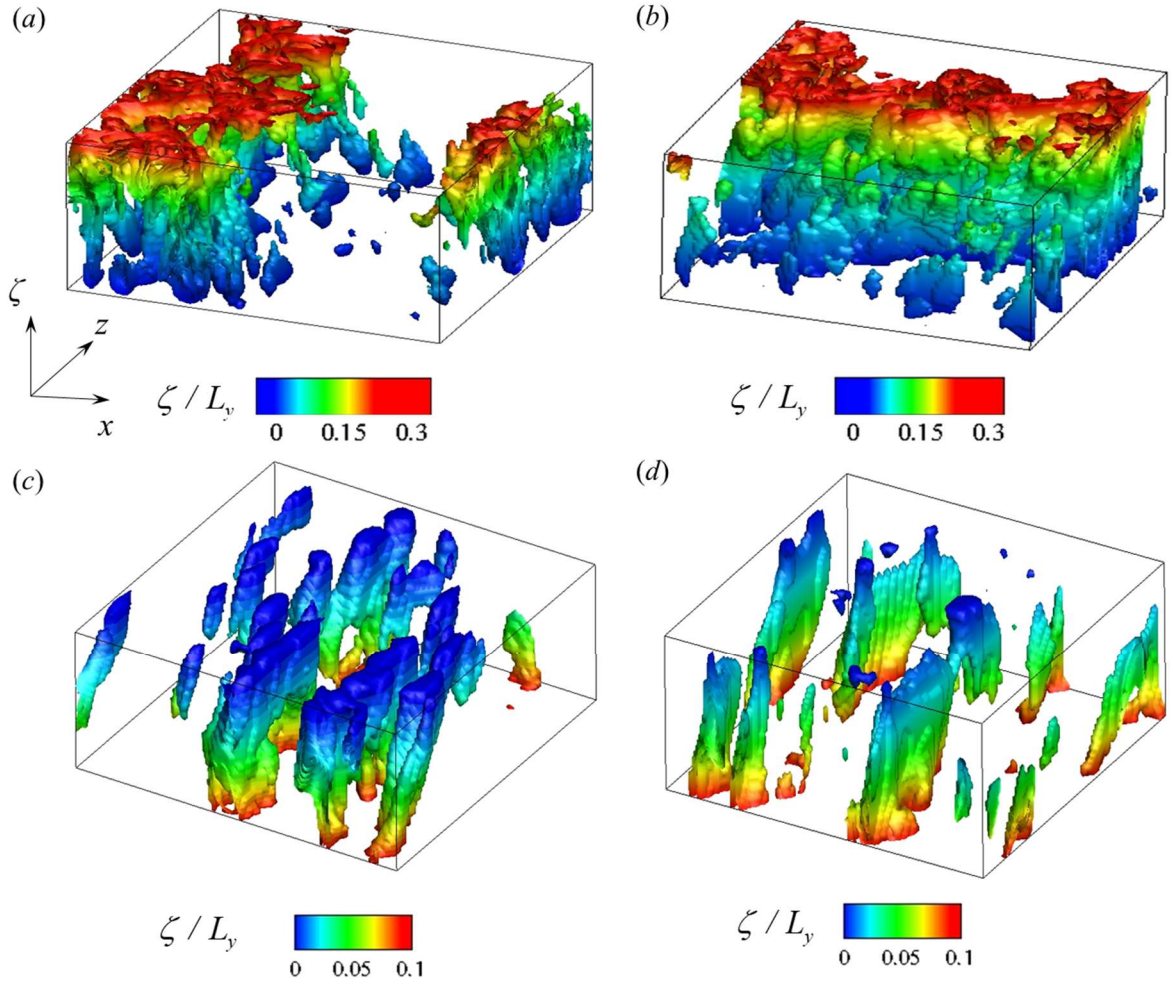

FIG. 10. Clusters of streamwise velocity fluctuations for TR3. The attached structures are distinguished based on Eqs. (23) and (24). (a) positive attached structures near the cold wall; (b) negative attached structures near the cold wall; (c) positive attached structures near the hot wall; (d) negative attached structures near the hot wall. The color indicates the distance from the wall. The wall-normal coordinate corresponds to $0 < \zeta^* < 100$, and the x and z axes show the whole streamwise and spanwise extents of the flow field.

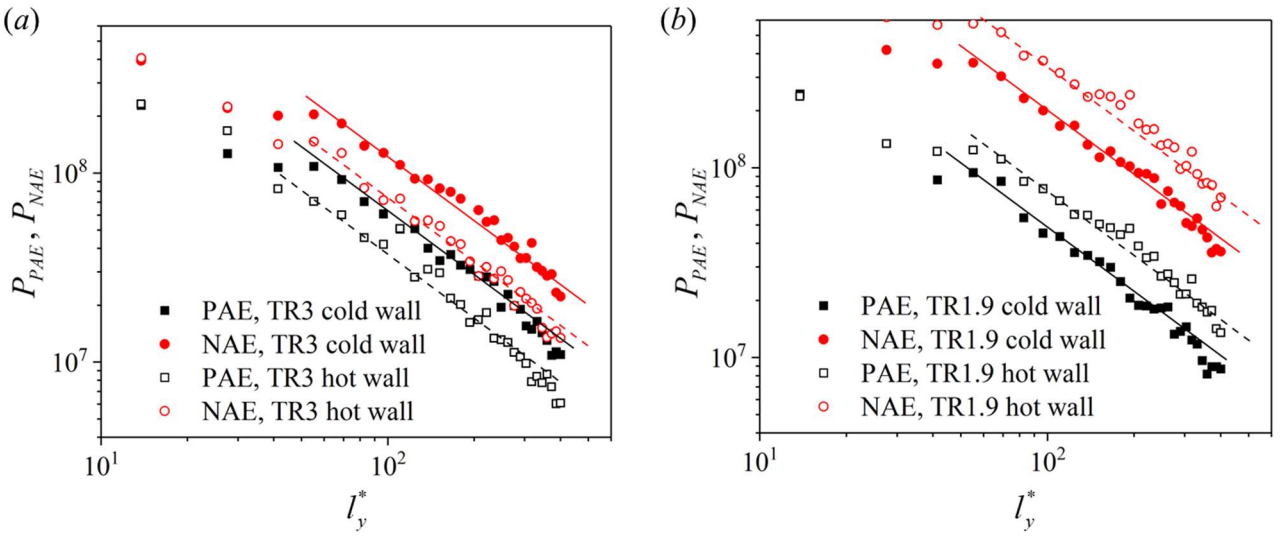

FIG. 11. Population density P ($P = N/(L_xL_z)$) of the positive and negative attached eddies as a function of their wall-normal extents l_y^*. (a) for TR3 and (b) for TR1.9. The straight lines denote the scaling $P \propto \left(l_y^*\right)^{-1.1}$.

In summary, we have proposed an extended attached eddy model in the context of transcritical thermodynamic conditions in this section. Compared with the classical attached eddy model [29] and the hierarchical random additive process model [34, 35, 50], we generalize the expression of the two-point velocity correlation by taking account of the characteristic velocity and mixed scaling for transcritical thermodynamic flows. The model yields the inverse wavenumber scaling of energy spectra and the $\left(\zeta^*\right)^{-1}$ scaling of population density of the eddies, which can be confirmed from DNS results. The mixed scaling reflecting the interactions within turbulent boundary layers enables the model to predict the statistics in transcritical boundary layers more accurately.

IV. CONCLUSIONS

In this work, we study the physical underpinning of the interactions within the turbulent boundary layer at transcritical conditions, and propose the characteristic scales and models of attached eddies. These observations are constructive for the development of the more accurate wall models of WMLES.

The conclusions are summarized as follows.

i) Remarkable coherence between the turbulence in the inner layer and the outer layer is found. The streamwise Reynolds stresses of fluctuating energy amplifies in the outer layer while decrease in the inner layer, which results from the energy transfer from the inner layer to the outer layer under real-fluid thermodynamic conditions. The interactions between the inner layer and the outer layer are highlighted by the success of mixed scaling that collapses energy spectra at transcritical conditions.

ii) The complicated coupling effects of the near-wall cycle and the wall-normal coherent motions (i.e., sweep and ejection) play significant roles in the interactions and energy transport within transcritical turbulent boundary layers. With decreasing density changes, ejection and sweep motions in turbulent boundary layers in the channel attenuate.

iii) The interactions within the boundary layers also modulate the characteristic velocity and lengthscale of the attached eddies in transcritical flows. It is found that the classical characteristic scales for attached eddies in incompressible flows cannot accurately characterize the attached eddies in turbulent boundary layers at transcritical conditions. An improved algebraic mixing length that can be employed as the reduced-order wall model in WMLES is proposed in the present work. This mixing-length model incorporates a modification of the semilocal scaling by the mixed scaling L_y/δ_v^*. We apply this mixing-length model in the log-layer at transcritical conditions and find that this model performs considerably well.

iv) Finally, an extended model for the wall-attached eddy at transcritical conditions is proposed in order to incorporate the interactions within the turbulent boundary layers in the attached eddy theory. The two-point correlation of fluctuating velocity induced by the attached eddy is established taking account of the new mixed scaling, and the extended attached eddy model can yield the celebrated

inverse wavenumber scaling of the streamwise energy spectra at transcritical conditions. Furthermore, the model predicts that the population density of attached eddies exhibits $P \propto \left(l_y^*\right)^{-1}$, with l_y^* the semilocally wall-normal extent of the eddies. This prediction agrees reasonably well with the DNS results.

ACKNOWLEDGMENTS

F.L. is funded by National Natural Science Foundation of China (Grant No. 92152301), China Postdoctoral Science Foundation (Grant No. 2023M742845), National Funded Postdoctoral Research Project (Grant No. GZB20230978) and Science and Technology Plan Project of Shaanxi Province (Grant No. 2024JC-YBQN-0010). M.I. is funded by U.S. Department of Energy Office of Science with Award DE-SC0022222. We thank Dr. Jack Guo from Lawrence Livermore National Laboratory for his helpful recommendations.

APPENDIX A. COMPARISON OF ATTACHED EDDY MODEL WITH CONSTANT-PROPERTY RESULTS

We show that the generalized derived model in Sec. III C can reduce to Townsend's wall-attached model for incompressible flows. For incompressible flow, Eq. (14) reduces to

$$\overline{\boldsymbol{u}''(\boldsymbol{x})\boldsymbol{u}''(\boldsymbol{x}+\boldsymbol{r})} = \int P(\boldsymbol{x}_a) u_\tau \frac{L_y^2}{\delta_v^2} \boldsymbol{f}\left(\frac{\boldsymbol{x}-\boldsymbol{x}_a}{\delta_v}\right) \boldsymbol{f}\left(\frac{\boldsymbol{x}+\boldsymbol{r}-\boldsymbol{x}_a}{\delta_v}\right) \mathrm{d}\boldsymbol{x}_a \tag{A1}$$

The eddy intensity function for incompressible flow reduces to

$$\boldsymbol{I}\left(0, \boldsymbol{x}^+\right) = \iint \boldsymbol{f}\left(\frac{\boldsymbol{x}-\boldsymbol{x}_a}{\delta_v}\right) \boldsymbol{f}\left(\frac{\boldsymbol{x}-\boldsymbol{x}_a}{\delta_v}\right) \mathrm{d}x_a^+ \mathrm{d}z_a^+ = \text{const} \tag{A2}$$

and

$$f_u \propto \frac{1}{\delta_v} g_u,\ f_v \propto \frac{\zeta}{\delta_v^2} g_v, \tag{A3}$$

with g being some function of $\left(x - x_a\right)/\delta_v$ and $\left(z - z_a\right)/\delta_v$. Thus, the extended attached eddy model yields the following scaling for streamwise velocity fluctuations for incompressible flows,

$$\frac{\overline{u''^2}}{u_\tau^2} \propto \int_\zeta^{L_y} N\left(\zeta_a\right) \mathrm{d}\zeta_a = A_1 \ln\left(L_y/\zeta\right) + B_1, \tag{A4}$$

which is consistent with $\overline{u''^2}/u_\tau^2$ obtained by the incompressible wall-attached eddy theory.

REFERENCES

[1] G. Simeoni, T. Bryk, F. Gorelli, M. Krisch, G. Ruocco, M. Santoro, and T. Scopigno, The Widom line as the crossover between liquid-like and gas-like behaviour in supercritical fluids, Nat. Phys. 6, 503 (2010).

[2] D. Bolmatov, V. Brazhkin, and K. Trachenko. Thermodynamic behavior of supercritical matter, Nat. Commun. 4, 2331 (2013).

[3] Guo, J., Yang, X. I. A. and Ihme, M. Structure of the thermal boundary layer in turbulent channel flows at transcritical conditions, J. Fluid Mech. 934, A45 (2022).

[4] P. C. Ma, X. I. A. Yang, and M. Ihme. Structure of wall-bounded flows at transcritical conditions, Phys. Rev. Fluids 3, 034609 (2018).

[5] F. B. Li, J. Guo, B. F. Bai, and M. Ihme. Analysis of real-fluid thermodynamic effects on turbulent statistics in transcritical channel flows, Phys. Rev. Fluids 8, 024605 (2023).

[6] F. B. Li, W. W. Zhang, B. F. Bai, and M. Ihme. Small-scale turbulent characteristics in transcritical wall-bounded flows, J. Fluid Mech. 986, A36 (2024).

[7] J. Y. Yoo, The turbulent flows of supercritical fluids with heat transfer. Annu. Rev. Fluid Mech. 45, 495 (2013).

[8] J. H. Bae, J. Y. Yoo, and H. Choi. Direct numerical simulation of turbulent supercritical flows with heat transfer. Phys. Fluids 17, 105104 (2005).

[9] J. H. Bae, J. Y. Yoo, and D. M. McEligot. Direct numerical simulation of heated CO_2 flows at supercritical pressure in a vertical annulus at Re = 8900. Phys. Fluids 20, 055108 (2008).

[10] J. W. R. Peeters, R. Pecnik, M. Rohde, T. H. J. J. van der Hagen, and B. J. Boersma, Turbulence attenuation in simultaneously heated and cooled annular flows at supercritical pressure, J. Fluid Mech. 799, 505 (2016).

[11] K. Kim, J. P. Hickey, and C. Scalo. Pseudophase change effects in turbulent channel flow under transcritical temperature conditions, J. Fluid Mech. 871, 52 (2019).

[12] R. R. Zhao and A. J. Smits. Scaling of the wall-normal turbulence component in high-Reynolds-number pipe flow, J. Fluid Mech. 576, 457 (2007).

[13] M. Guala, M. Metzger, and B. J. Mckeon. Interactions within the turbulent boundary layer at high Reynolds number, J. Fluid Mech. 666, 573 (2011).

[14] S. J. Kline, W. C. Reynolds, F. A. Schraub, and P. W. Runstadler. The structure of turbulent boundary layers. J. Fluid Mech. 30, 741 (1967).
[15] A. J. Smits, B. J. McKeon, and I. Marusic. High-Reynolds number wall turbulence. Annu. Rev. Fluid Mech. 43, 353 (2011).
[16] R. J. Adrian, C. D. Meinhart, and C. D. Tomkins. Vortex organization in the outer region of the turbulent boundary layer. J. Fluid Mech. 422, 1 (2000).
[17] I. Marusic, G. J. Kunkel, and F. Porte-Agel. Experimental study of wall boundary conditions for large-eddy simulation. J. Fluid Mech. 446, 309 (2001).
[18] J. P. Monty, J. A. Stewart, R. C. Williams, and M. S. Chong. Large-scale features in turbulent pipe and channel flows. J. Fluid Mech. 589, 147 (2007).
[19] X. Wu and P. Moin, Forest of hairpins in a low-Reynolds-number zero-pressure-gradient flat-plate boundary layer. Phys. Fluids 21, 091106 (2009).
[20] S. Deng, C. Pan, J. J. Wang and G. S. He. On the spatial organization of hairpin packets in a turbulent boundary layer at low-to-moderate Reynolds number. J. Fluid Mech. 844, 635 (2018).
[21] J. C. R. Hunt and J. F. Morrison. Eddy structure in turbulent boundary layers. European J. Mech. 19, 673 (2000).
[22] J. C. R. Hunt and P. Carlotti. Statistical structure at the wall of the high Reynolds number turbulent boundary layer. Flow Turbul. Combust. 66, 453 (2001).
[23] U. Hogstrom, U., J. C. R. Hunt, and A. S. Smedman. Theory and measurements for turbulence spectra and variances in the atmospheric neutral surface layer. Boundary-Layer Meteorology, 103, 101 (2002).
[24] M. Lee and R. D. Moser. Direct numerical simulation of turbulent channel flow up to $Re_\tau \sim 5200$. J. Fluid Mech. 774, 395 (2015).
[25] B. Ganapathisubramani, E. K. Longmire, I. Marusic, and S. Pothos. Dual-plane PIV technique to determine the complete velocity gradient tensor in a turbulent boundary layer. Exp. Fluids, 39, 222 (2005).
[26] G. Wang and X. Zheng. Very large scale motions in the atmospheric surface layer: A field investigation. J. Fluid Mech. 802, 464 (2016).
[27] C. Cheng and L. Fu. Consistency between the attached-eddy model and the inner-outer interaction model: a study of streamwise wall-shear stress fluctuations in a turbulent channel flow, J. Fluid Mech. 942, R9 (2022).
[28] J. F. Morrison, B. J. McKeon, W. Jiang, and A. J. Smits. Scaling of the streamwise velocity component in turbulent pipe flow, J. Fluid Mech. 508, 99 (2004).
[29] A. A. Townsend, The Structure of Turbulent Shear Flow. Cambridge University Press, 1976.
[30] I. Marusic, J. P. Monty, M. Hultmark, and A. J. Smits. On the logarithmic region in wall turbulence. J. Fluid Mech. 716, R3 (2013).
[31] A. Lozano-Durán and H. J. Bae. Characteristic scales of Townsend's wall-attached eddies. J. Fluid Mech. 868, 698 (2019).
[32] J. Hwang and H. J. Sung. Wall-attached structures of velocity fluctuations in a turbulent boundary layer, J. Fluid Mech. 856, 958 (2018).
[33] I. Marusic and J. P. Monty. Attached eddy model of wall turbulence. Annu. Rev. Fluid Mech. 51, 49 (2019).
[34] A. E. Perry, and M. S. Chong. On the mechanism of wall turbulence. J. Fluid Mech. 119, 173 (1982).

[35] A. E. Perry, S. Henbest, and M. S. Chong, A theoretical and experimental study of wall turbulence. J. Fluid Mech. 165, 163 (1986).
[36] A. E. Perry, and I. Marusic. A wall-wake model for the turbulence structure of boundary layers. Part 1. Extension of the attached eddy hypothesis. J. Fluid Mech. 298, 361 (1995).
[37] I. Marusic and G. J. Kunkel. Streamwise turbulence intensity formulation for flat-plate boundary layers. Phys. Fluids 15, 2461 (2003).
[38] Y. Hwang and B. Eckhardt. Attached eddy model revisited using a minimal quasi-linear approximation, J. Fluid Mech. 894, A23 (2020).
[39] I. Marusic, W. J. Baars, N. Hutchins. Scaling of the streamwise turbulence intensity in the context of inner-outer interactions in wall-turbulence. Phys. Rev. Fluids, 2, 100502 (2017).
[40] C. Cheng, W. P. Li, A. Lozano-Duran, and H. Liu. Uncovering Townsend's wall-attached eddies in low-Reynolds-number wall turbulence, J. Fluid Mech. 889, A29 (2020).
[41] R. F. Hu, X. I. A. Yang, and X. J. Zheng. Wall-attached and wall-detached eddies in wall-bounded turbulent flows, J. Fluid Mech. 885, A30 (2020).
[42] A. Patel, J. W. R. Peeters, B. J. Boersma, and R. Pecnik. Semi-local scaling and turbulence modulation in variable property turbulent channel flows, Phys. Fluids 27, 095101 (2015).
[43] A. Patel, B. J. Boersma, and R. Pecnik. The influence of near-wall density and viscosity gradients on turbulence in channel flows, J. Fluid. Mech. 809, 793 (2016).
[44] A. Patel, B. J. Boersma, and R. Pecnik. Scalar statistics in variable property turbulent channel flows, Phys. Rev. Fluids 2, 084604 (2017).
[45] S. Kawai. Heated transcritical and unheated non-transcritical turbulent boundary layers at supercritical pressures. J. Fluid Mech. 865, 563 (2019).
[46] D. Y. Peng and D. B. Robinson, A new two-constant equation of state, Ind. Eng. Chem. Fund. 15, 59 (1976).
[47] T. H. Chung, M. Ajlan, L. L. Lee, and K. E. Starling. Generalized multiparameter correlation for nonpolar and polar fluid transport properties, Ind. Eng. Chem. Fund. 27, 671 (1988).
[48] W. J. Baars, N. Hutchins, and I. Marusic. Self-similarity of wall-attached turbulence in boundary layers. J. Fluid Mech. 823, R2 (2017).
[49] P. C. Ma, T. Ewan, C. Jainski, L. Lu, A. Dreizler, V. Sick, and M. Ihme. Development and analysis of wall models for internal combustion engine simulations using high-speed Micro-PIV measurements, Flow Turbul. Combust. 98, 283 (2017).
[50] H. Mouri. Two-point correlation in wall turbulence according to the attached-eddy hypothesis. J. Fluid Mech. 821, 343 (2017).